

# OJ 287: a new BH mass estimate of the secondary

Lev Titarchuk<sup>1</sup>, Elena Seifina<sup>2</sup>, and Chris Shrader<sup>3,4</sup>

<sup>1</sup> Dipartimento di Fisica, University di Ferrara, Via Saragat 1, I-44122, Ferrara, Italy, e-mail: titarchuk@fe.infn.it,

<sup>2</sup> Lomonosov Moscow State University/Sternberg Astronomical Institute, Universitetsky Prospect 13, Moscow, 119992, Russia, e-mail: seif@sai.msu.ru

<sup>3</sup> NASA Goddard Space Flight Center, NASA, Astrophysics Science Division, Code 661, Greenbelt, MD 20771, USA, e-mail: Chris.R.Shrader@nasa.gov

<sup>4</sup> Universities Space Research Association, 10211 Wincopin Cir, Suite 500, Columbia, MD 21044, USA

Received, January 17, 2023, accepted February 11, 2023

## ABSTRACT

We presented a study of outburst activity in the BL Lacertae source OJ 287, observed extensively with the X-ray telescope (XRT) onboard Neil Gehrels Swift Observatory. We demonstrated that the results of our analysis of X-ray flaring activity using the Swift/XRT data allow to refine the key characteristics of the OJ 287 secondary (its nature and mass). We discovered that the energy spectra in all spectral states can be fitted using the XSPEC Bulk Motion Comptonization (BMC) model. As a result we found that the X-ray photon index of the BMC model,  $\Gamma$  correlates with the mass accretion rate,  $\dot{M}$ . We established that  $\Gamma$  increases monotonically with  $\dot{M}$  from the low-hard state,  $\Gamma \sim 1.5$  to the high-soft state,  $\Gamma \sim 2.8$  and finally saturates. The index behavior was similar to that in a number of black hole (BH) candidates in which we showed that its saturation was an observational evidence of the presence of a BH. Based on this correlation, we applied a scaling method and determined that a secondary BH mass in OJ 287 is about  $\sim 1.25 \times 10^8$  solar masses, using the well-studied X-ray BH binaries XTE 1550–564, H 1743–322, 4U 1630–47, GRS 1915+105 as well as extragalactic BHs ESO 243–49 and M101 ULX–1, as reference sources. Also using the power spectrum analysis we inferred the size of the Compton cloud  $L_{CC} \sim 10^{13}$  cm where X-ray spectra were formed. Using this value of  $L_{CC}$  we confirmed that a BH mass of the secondary in OJ 287 was of order of  $10^8$  solar masses as we derived using the index,  $\Gamma$ –correlation (the scaling method) with respect of the mass accretion rate.

**Key words.** accretion, accretion disks – black hole physics – stars, galaxies: active – galaxies: Individual: OJ 287 – radiation mechanisms

## 1. Introduction

Galaxy OJ 287 is a BL Lacertae object (blazar) in the constellation Cancer and is located at a distance of five billion light years from Earth. As is known, blazars are associated with a supermassive black hole (SMBH), which collects the surrounding matter, dust and gas, forming an accretion disk. However, OJ 287 is interesting not only for this. At its center is not one, but two SMBHs (Gomes et al. 2022; Dou et al. 2022). These two black holes form an orbital pair located in the core of this galaxy. This pair is the only close binary system of two SMBHs known to date (Valtonen et al. 2006; Laine et al. 2020; Gomes et al. 2022). In turn, a large black hole (primary) has a mass equal to 18 billion solar masses, in fact equal to the mass of a small galaxy. The less massive black hole (secondary) weighs as much as 100 million solar masses. In addition, the secondary revolves around the primary (see Fig. 1), piercing/drilling through its accretion disk twice every 12 years (Shi et al. 2007; Dey et al. 2019). SMBHs binaries are an amazing by-product of galaxy mergers in a hierarchical universe (Begelman et al. 1980). In the last stage of their orbital evolution, gravitational wave radiation provides the binary inspiral. Periodically varying radiation from active galactic nuclei has been proposed as a powerful tool for studying such binary systems (Chen et al. 2020; Charisi et al. 2016; Liu et al. 2016; Zheng et al. 2016; Graham et al. 2015).

The goal of our paper is to check a mass value of the secondary black hole (BH) in OJ 287 applying the scaling method for a BH mass determination [Shaposhnikov & Titarchuk

(2009), hereafter ST09] based on observations during source X-ray outbursts. Because OJ 287 exhibited a more or less strict 12-year cycle, several hypotheses have been proposed to explain the optical/X-ray periodic variability of the object (Sillanpaa et al. 1988; Shi et al. 2007). In particular, according to Valtonen et al. (2012), hereafter V12, the periodicity is presumably due to the orbital rotation of the components in a BH binary, in which the secondary periodically perturbs the accretion disk around the primary.

V12 presented results of the two X-ray observations of OJ 287 by XMM–Newton in 2005 April 12 and November 3–4. V12 claimed that the spectral energy distribution, the spectrum from radio to X-rays on April 12, 2005 followed nicely a synchrotron self-Compton (SSC) model [see Ciprini et al. (2007)]. In contrast, the November 3–4 spectrum was quite different. The flux rose prominently in the optical/UV region, but in the radio or hard X-rays the flux remained at the pre-outburst level, making the single zone SSC model unlikely. However, V12 model of the optical/UV outburst in the context of an interaction between the secondary and the primary accretion disk leading to a mass estimate of  $M_{sec} \sim 1.4 \times 10^8 M_{\odot}$ . V12 also formulated a question regarding the primary BH mass in order it could guarantee the stability of the primary accretion disc. They found that the minimum value of the primary mass  $1.8 \times 10^{10} M_{\odot}$  is quite close to the BH mass determined from the orbit solution technique,  $1.84 \times 10^{10} M_{\odot}$ .

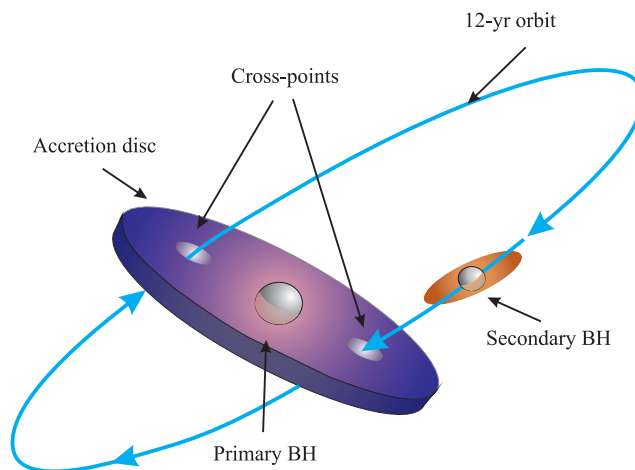


**Fig. 1.** A schematic view of OJ 287 model used in our analysis.

To find evidence for the emission of the secondary, V12 needed to look at short time-scale variability in OJ 287. It has been found to be variable from 15 min time-scale upwards on many occasions [see for example, Gupta et al. (2012)] and on one occasion the light curve has shown sinusoidal variations of the period of 228 min (Sagar et al. 2004). If this variation is associated with the last stable orbit of a maximally rotating black hole, the mass of the black hole is  $1.46 \times 10^8 M_{\odot}$  (Gupta et al. 2012), i.e. identical to the mass obtained from the orbit solution (Valtonen et al. 2010).

Komossa et al. (2021), hereafter KOM21 made a detailed analysis of XMM–Newton spectra of OJ 287 spreading 15 yr. KOM21 also presented their achieved findings from *Swift* UVOT and XRT observation of OJ 287, which begun in 2015, along with all public *Swift* information after 2005. During this period, OJ 287 was found in an “*extreme*” low-hard state (LHS) and outburst high-soft states (HSS). In addition, they established that the OJ 287 X-ray spectra were highly variable and passed all states seen in blazars from a “*flat*” LHS through an intermediate state (IS) to exceptionally a soft steep (ST) state. KOM21 found that these spectra can be made up using the following parts: Inverse Compton (IC) radiation which is prevailing in the LHS, very soft radiation that turned into extremely powerful when OJ 287 became more luminous. KOM21 claimed that their 2018 XMM–Newton measurements, almost contemporary with the EHT examination of OJ 287, were well characterized by a model with a hard IC component with the photon index  $\Gamma \sim 1.5$  and a soft component. It is important to emphasize that they concluded that the LHS spectra limited any long-lived accretion disc/corona contribution in X-rays and related to a very low value of  $L_x/L_{Edd} < 5.6 \times 10^{-4}$  (for  $M_{BH}$  of the primary  $\sim 1.8 \times 10^{10} M_{\odot}$ ).

We are suggesting a revision of this claim by KOM21 reanalyzing data of X-ray telescope (XRT) onboard of *Swift* observatory for OJ 287 and applying the ST09 scaling method to these data in order to make a BH mass estimate. Using this method requires an accurate knowledge of the distance to the source OJ 287. The method was proposed back in 2007 by Shaposhnikov & Titarchuk (2007), hereafter ST07 and by ST09. It is worth noting that there are two scaling methods: based on the correlation between the photon index,  $\Gamma$  and the quasi-periodic oscillation (QPO) frequency,  $\nu_L$ ; and one based on the correlation between  $\Gamma$  and normalization of the spectrum proportional to  $\dot{M}$ . If for the first method ( $\Gamma - \nu_L$ ) to estimate a BH mass the

distance to the source is not required (ST07), while for the second method,  $\Gamma - \dot{M}$  (see ST09) the source distance and the inclination of the accretion disk relative to the Earth observer are needed.

For both methods, it is necessary that the source shows a change in spectral states during the outburst and a characteristic behavior of  $\Gamma$ . A monotonic increase of  $\Gamma$  with  $\nu_L$  or  $\dot{M}$  in the LHS→IS→HSS transition and reaching a constant level (saturating) at high values of  $\nu_L$  or  $\dot{M}$ . Then  $\Gamma$  monotonic decreases during HSS→IS→LHS transition when the outburst decay. The saturation of  $\Gamma$  (so-called “ $\Gamma$ -saturation phase”) during outburst is a specific signature that this particular object contains a BH (Titarchuk & Zannias 1998). Indeed, the  $\Gamma$ -saturation phase can be caused only by an accretion flow converging to the event horizon of a BH (see the Monte-Carlo simulation results in Laurent & Titarchuk (1999, 2011)). Then, it makes sense to compare BH sources that have the same  $\Gamma$ -saturation levels. In the second method ( $\Gamma - \dot{M}$ ), it is assumed that BH luminosity is directly proportional to  $\dot{M}$  (and, consequently, to the mass of the central BH), and inversely proportional to the squared distance to the source. Thus, we can determine the BH mass by comparing the corresponding tracks  $\Gamma - \dot{M}$  for a pair of sources with BHs, in which all parameters are known for one source, and for the other source parameters except a BH mass are known (for more details on the scaling method, see Titarchuk et al. (2010); Seifina & Titarchuk (2010) and ST09).

The scaling method has a number of advantages in determination of a BH mass, compared to other methods. Calculation of the X-ray spectrum originating in the innermost part of the source based on first-principle (fundamental) physical models, taking into account the Comptonization of the soft disk photons by hot electrons of internal disk part and in a converging flow to a BH. In fact, in the case of a  $10^8 M_{\odot}$  BH the disk peak temperature is relatively low,  $kT_s < 1 \text{ keV}/(M_{BH}/10M_{\odot})^{1/4}$ , i.e. about 20–100 eV and its thermal peak is in the UV energy range [see details of our observation in §3 and Shakura & Sunyaev (1973)]. It is worth noting that using this scaling method for a BH mass estimate Titarchuk & Seifina (2016a); Seifina et al. (2017); Titarchuk & Seifina (2017); Seifina et al. (2018a,b); Titarchuk et al. (2020) applied it to intermediate mass BHs and SMBHs.

In this paper, based on *Swift* data analysis, we estimate a BH mass in OJ 287 using the scaling technique. In §2 we provide details of our data analysis, while in §3 we present a description

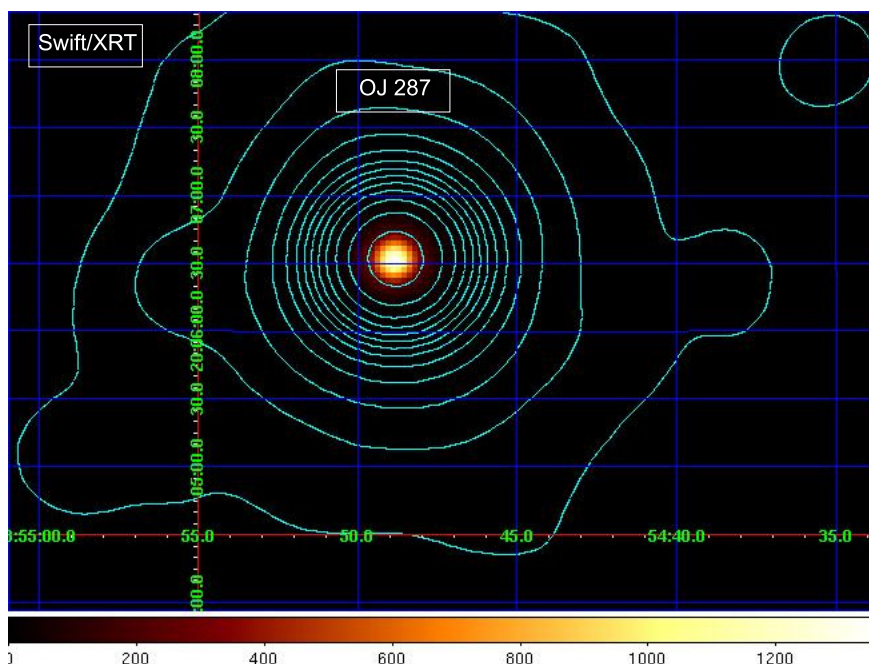


**Fig. 2.** A *Swift* X-ray image on May 20, 2005 – June 13, 2018 with 455 ks exposure. Contours correspond to fourteen logarithmic intervals with respect to the brightest pixel.

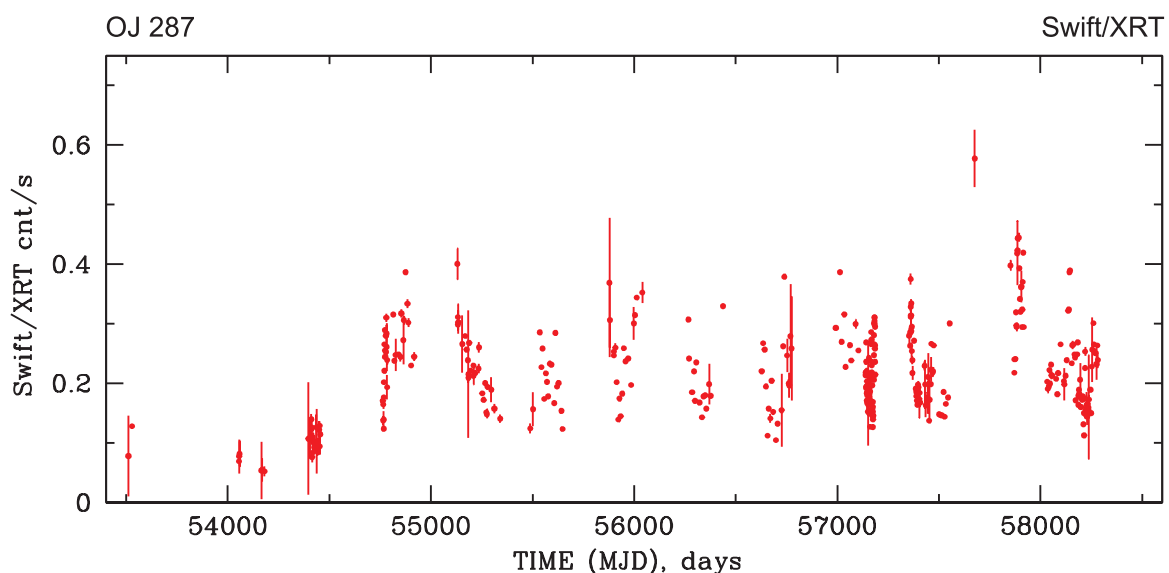


**Fig. 3.** Evolution of XRT/*Swift* count rate during the 2005 – 2018 observations of OJ 287.

of the spectral models used for fitting these data. In §4 we focus on the interpretation of our observations. In §5 we focused on the construction of the power density spectra (PDS) and its interpretation. In §6 we discuss the main results of the paper. In §7 we present our final conclusions.

## 2. Data Reduction

Using *Swift*/XRT data in 0.3–10 keV energy range we studied a total of 385 observations of OJ 287 during its flaring events from 2005 to 2018. The data used in this paper are public and available through the GSFC public archive at <https://heasarc.gsfc.nasa.gov>. In Table 1 we report the log of observations for OJ 287 used in our study. We must admit that not all of the flare events may related to the secondary BH – disk in-

teractions. Thus, it may be challenging to disentangle them from other flaring that goes on in OJ 287 all the time, completely unrelated to any binary’s presence.

Data were processed using the HEASOFT v6.14, the tool *xrtpipeline* v0.12.84 and the calibration files (CALDB version 4.1). The ancillary response files were created using *xrtmkarf* v0.6.0 and exposure maps generated by *xrtexpomap* v0.2.7. Source events were accumulated within a circular region with radius of 47” centered at the position of OJ 287 [ $\alpha = 08^h58^m47^s.15$  and  $\delta = +20^{\circ}08'00''.5$ , J2000.0]. We used XRT data both in the Windowed Timing (WT) mode ( $\geq 1$  count/s) and in the Photon Counting mode for the remaining observations when the X-ray source became sufficiently faint. The background was estimated in a nearby source-free circular region of 118” radius.

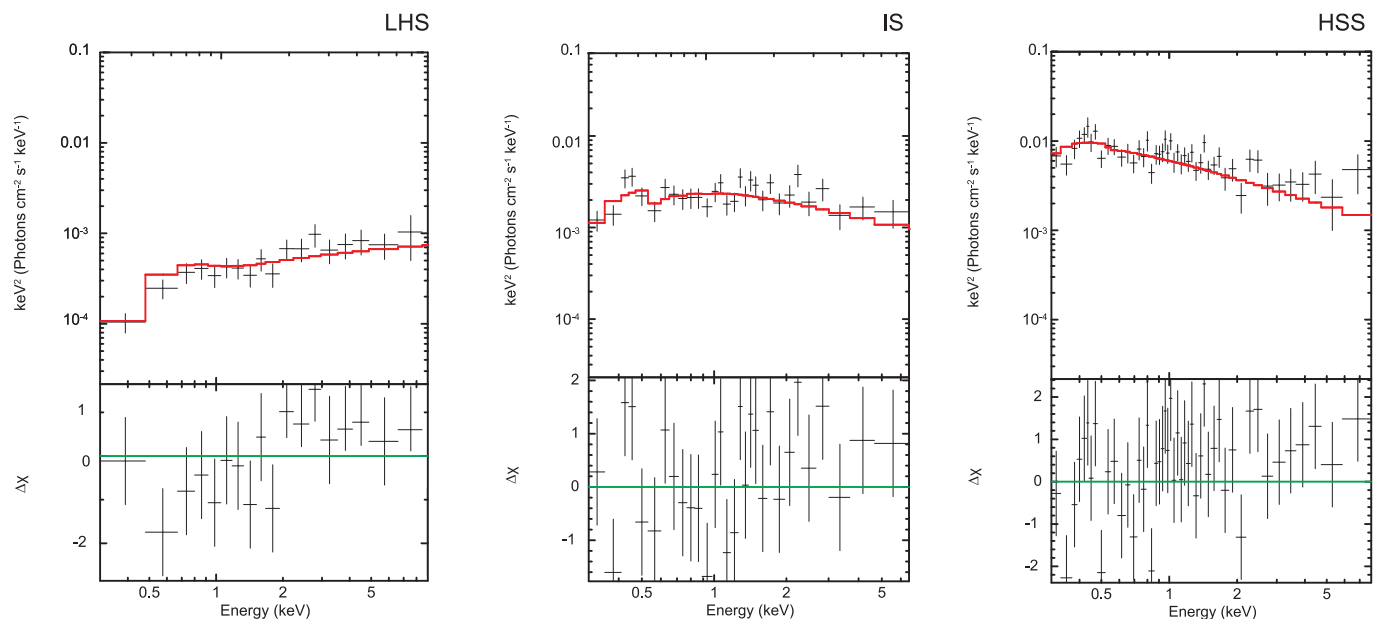


**Fig. 4.** Three representative spectra of OJ 287 from *Swift* data with best-fit modelling for the LHS (ID=00035011001), IS (ID=00088085001) and HSS (ID=00034934051) states in units  $E * F(E)$  using `tbabs*bmc` model. The data are denoted by *black* crosses, while the spectral model presented by *red* histogram.

**Table 1.** The list of *Swift* observations of OJ 287 used in our analysis

Obs. ID	Start time (UT)	End time (UT)	MJD interval
00020117001	2009 October 28 17:05:58	2009 October 29	55132.7 – 55132.8
00030901(001-002,004-015,017-026,029-039, 041-048,050-051,053-061,063-064,066-067, 069,071-089,091,093-099,101-109,111-117, 119-122,124-128,130-146,148-150,152-155, 157-162,164-165,167-178,181-196,198-215, 217,219-220)	2007 March 6	2016 Oct 15	54165 – 57676
00035011(001,003)	2005 May 20	2005 June 7	53510 – 53528
00035905(001-003)	2006 Nov 16	2006 Nov 18	54055.6 – 54026
00090015(002-012)	2008 Oct 24	2009 Sep 16	54763 – 55090
00090086(001-003)	2010 Jan 13	2010 Mar 23	55209 – 55728
00033756(002-020,022-068,073,075-086,088-089)	2015 Apr 28	2015 Jun 14	57140 – 57187
00034934(051-053,055-070,072-080,082-083, 086-089,091,093-096,098-113,115-123,125 127-143,145-147)	2017 Feb 15	2018 Jun 13	57799 – 58282
00088085(001)	2017 Apr 9 16:18:13	18:06:53	57852 – 57852.7
00088667001	2018 Apr 20 15:35:14	17:15:53	58228 – 58228.7

Using the `xselect v2.4` task, source and background light curves and spectra were generated. Spectra were re-binned with at least 10 counts in in each energy bin using the `grppha` task in order to apply  $\chi^2$ -statistics. We also used the online XRT data product generator<sup>1</sup> to obtain the image of the source field of view in order to make a visual inspection and to get rid of a possible contamination from nearby sources (Evans et al. 2007, 2009). *Swift*/XRT (0.3 – 10 keV) image of OJ 287 field of view is presented in Fig. 2 and demonstrates absence of the X-ray jet-like (elongated) structure as well as the minimal contamination by other point sources and diffuse emission within a region of 120'' radius around OJ 287. We used *Swift* observation of OJ 287 (2005 – 2018) extracted from the HEASARC archives and found that these data cover a wide range of X-ray luminosities.

Before to proceeding with details of the spectral fitting we study a long-term behavior of OJ 287, in particular, its activity patterns. We present a long-term X-ray light curve of OJ 287 detected by the XRT onboard of the *Swift* over 2005 – 2018 (see Fig. 3).

Note, that this X-ray light curve makes it rather difficult to judge the 12-yr periodicity found earlier from optical observations. But it can be unequivocally stated that the object OJ 287 has become active over the past 10 years and shows sporadic X-ray activity (e.g., MJD 54500–58200, see Fig. 3).

### 3. Analysis and Results

In this section we present the results of spectral analysis during the outburst of OJ 287 observed by *Swift*/XRT. We analyze how the X-ray spectrum of the source behaves, in particular,  $\Gamma$  during the outburst.

<sup>1</sup> [http://www.swift.ac.uk/user\\_objects/](http://www.swift.ac.uk/user_objects/)

**Table 2.** BH masses and distances

Reference sources	$m_r$ ( $M_\odot$ )	$i_r^{(a)}$ (deg)	$N_r$ ( $L_{39}/d_{10}^2$ )	$d_r$ (kpc)
XTE J1550–564 <sup>(1)</sup>	$10.7 \pm 1.5$	72	1.	$3.3 \pm 0.5$
H 1743–322 <sup>(2)</sup>	$13.3 \pm 3.2$	70	0.19	$9.1 \pm 1.5$
4U 1630–47 <sup>(3)</sup>	$10 \pm 0.1$	70	0.12	$10 \pm 1$
ESO 243–49 <sup>(4)</sup>	$(7.2 \pm 0.7) \times 10^4$	75	$4.2 \times 10^{-6}$	$(95 \pm 10) \times 10^3$
M101 ULX-1 <sup>(5)</sup>	$(3.7 \pm 0.6) \times 10^4$	18	$3 \times 10^{-4}$	$(6.9 \pm 0.7) \times 10^3$
GRS 1915+105 <sup>(6)</sup>	$12.4 \pm 2$	70	0.2	$8.6 \pm 2$
Target source	$m_t$ ( $M_\odot$ )	$i_t^{(a)}$ (deg)	$d_t^{(b)}$ (kpc)	
OJ 287	$\sim 1.25 \times (1 \pm 0.45) \times 10^8$	50	1.037 Gpc	that using XTE J1550-564- as a reference source
OJ 287	$\sim 1.25 \times (1 \pm 0.45) \times 10^8$	50	1.037 Gpc	that using H 1743–322 as a reference source
OJ 287	$\sim 1.25 \times (1 \pm 0.45) \times 10^8$	50	1.037 Gpc	that using 4U 1630–47 as a reference source
OJ 287	$\sim 1.25 \times (1 \pm 0.45) \times 10^8$	50	1.037 Gpc	that using ESO 243-49 as a reference source
OJ 287	$\sim 1.25 \times (1 \pm 0.45) \times 10^8$	50	1.037 Gpc	that using M101-ULX-1 as a reference source
OJ 287	$\sim 1.25 \times (1 \pm 0.45) \times 10^8$	50	1.037 Gpc	that using GRS 1915+105 as a reference source
OJ 287	Final estimate	50	1.037 Gpc	as a standard deviation for a mean:
	$\sim 1.25 \times (1 \pm 0.18) \times 10^8$			$0.45/6^{1/2} = 0.18$

(a) System inclination in the literature and (b) source distance found in literature. (1) ST09; Orosz et al. (2002); Sanchez-Fernandez et al. (1999); Sobczak et al. (1999); (2) ST09; (3) Seifina et al. (2014); (4) Titarchuk & Seifina (2016b); (5) Titarchuk & Seifina (2016a) and (6) Titarchuk & Seifina (2009).

In our paper, we adhere to the scenario in which OJ 287 is a binary system consisting of two black holes with a larger and smaller mass (Fig. 1). In this case, a heavier BH (primary BH) is surrounded by a powerful accretion disk, and a lighter BH (secondary BH) orbits around the primary BH in a plane different from the equatorial plane of the primary BH accretion disk, crossing it twice during the orbital period (12 years). We also assume that when the secondary BH passes through the disk around the primary BH, “tidal disruption” of nearby parts of the disk occurs, due to which the partial disruption and subsequent matter replenishment of the accretion disk around the secondary BH is possible [see a similar process in Chan et al. (2021)]. In this case, a powerful transient disk develops around the secondary SBH with subsequent accretion of the material of the transient disk onto the secondary BH. This provides an increase in luminosity in the form of an outburst in the X-ray/optical/radio bands.

### 3.1. Spectral analysis

To fit the energy spectra of this source we used an XSPEC model consisting of the Comptonization (bulk-motion Comptonization, hereafter BMC) component [see Titarchuk & Zannias (1998); Laurent & Titarchuk (1999)]. We also use a multiplicative tbabs model (Wilms et al. 2000) which takes into account absorption by neutral material. We assume that accretion onto a BH is described by two main zones [see, for example, Fig. 1 in Titarchuk & Seifina (2021)]: a geometrically thin accretion disk (e.g. the standard Shakura-Sunyaev disk, see SS73 and a transition layer (TL), which is an intermediate link between the accretion disk, and a converging (bulk) region (see Titarchuk & Fiorito (2004)), that is assumed to exist, at least, below 3 Schwarzschild radii,  $3R_S = 6GM_{\text{BH}}/c^2$ . The spectral model parameters are the equivalent hydrogen absorption column density  $N_H$ ; the photon index  $\Gamma$ ;  $\log(A)$  is related to the Comptonized factor  $f [= A/(1+A)]$ ; the color temperature and normalization of the seed photon blackbody component,  $kT_s$  and  $N$ , respectively. The parameter  $\log(A)$  of the BMC component is fixed at 2 when the best-fit  $\log(A) \gg 1$ . In fact, for a sufficiently high  $\log(A) \gg 1$  (and, therefore, a high value  $A$ ), the illumination

factor  $f = A/(1+A)$  becomes a constant value close to 1 (that is, the same as in the case of  $\log(A) = 2$ ).  $N_H$  was fixed at the Galactic absorption level of  $2.49 \times 10^{20} \text{ cm}^{-2}$  (Wilms et al. 2000).

Similarly to the bbody XSPEC model, the normalization is a ratio of the source (disk) luminosity  $L$  to the square of the distance  $d$  (ST09, see Eq. 1 there):

$$N = \left( \frac{L}{10^{39} \text{ erg/s}} \right) \left( \frac{10 \text{ kpc}}{d} \right)^2. \quad (1)$$

This encompasses an important property of our model. Namely, using this model one can correctly evaluate normalization of the original “seed” component, which is presumably a correct  $\dot{M}$  indicator (Seifina & Titarchuk 2011). In its turn

$$L = \frac{GM_{\text{BH}}\dot{M}}{R_*} = \eta(r_*)\dot{m}L_{\text{Ed}}. \quad (2)$$

Here  $R_* = r_*R_S$  is an effective radius where the main energy release takes place in the disk,  $R_S = 2GM/c^2$  is the Schwarzschild radius,  $\eta = 1/(2r_*)$ ,  $\dot{m} = \dot{M}/\dot{M}_{\text{crit}}$  is the dimensionless  $\dot{M}$  in units of the critical mass accretion rate  $\dot{M}_{\text{crit}} = L_{\text{Ed}}/c^2$ , and  $L_{\text{Ed}}$  is the Eddington luminosity. For the formulation of the Comptonization problem one can see Titarchuk et al. (1997); Titarchuk & Zannias (1998); Laurent & Titarchuk (1999); Borozdin et al. (1999); Shaposhnikov & Titarchuk (2009).

Spectral analysis of the *Swift*/XRT data fits of OJ 287, in principle, provides a general picture of the source evolution. We can trace the change in the spectrum shape during the LHS–IS–HSS transition. In Figure 4, we show three representative  $E * F_E$  spectral diagrams for different states of OJ 287.

We put together spectra of the LHS, IS, and HSS, to demonstrate the source spectral evolution from the low-hard to high-soft to states based on the *Swift* observations. Data are presented here: at the left panel for LHS (taken from observation 00088085001), at the central panel for IS (00035011001) and at the right panel for the HSS (taken from observation 00034934051) in units  $E * F(E)$  fitted using tbabs\*bmc model. Periods of exposure are 3.7, 1.9 and 1.1 ks, respectively.

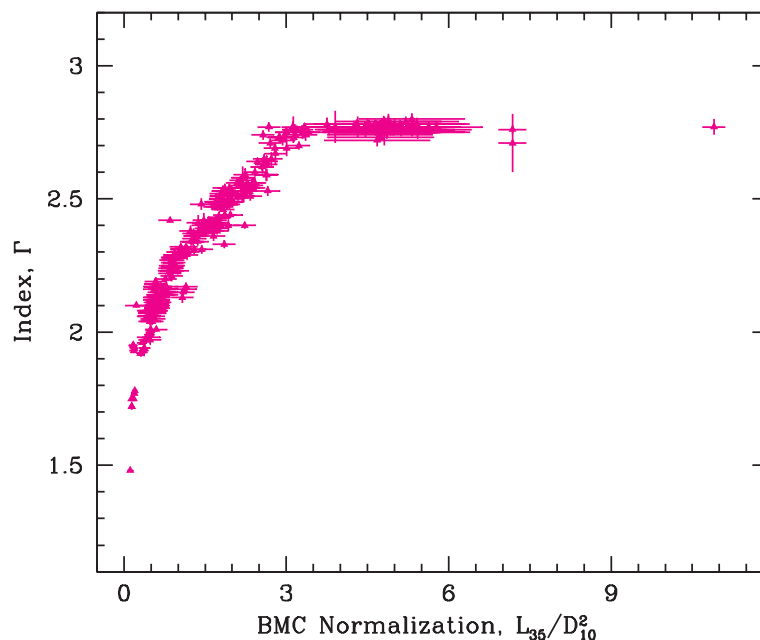


**Fig. 5.** Correlation of the photon index  $\Gamma$  ( $= \alpha + 1$ ) versus the BMC normalization,  $N$  (proportional to mass accretion rate) in units of  $L_{39}/D_{10}^2$ .

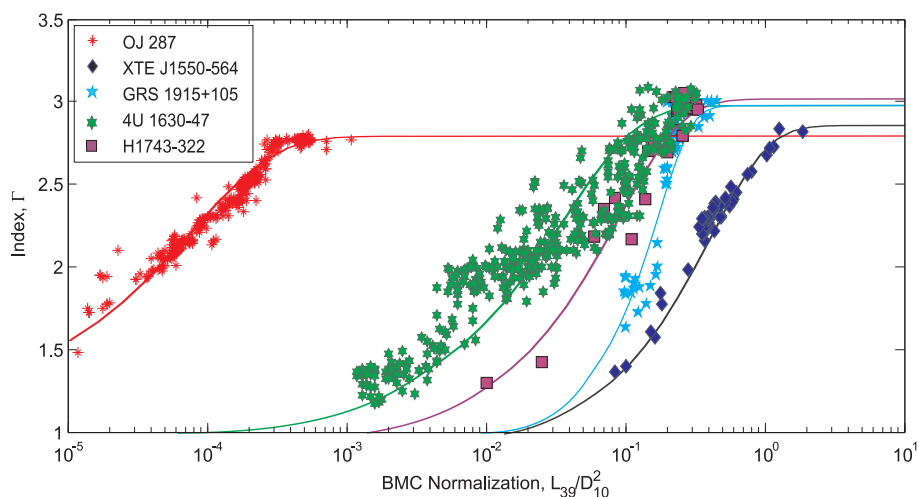


**Fig. 6.** Scaling of the photon index,  $\Gamma$  versus the normalization  $N_{BMC}$  for OJ 287 (red points – target source) using the correlation for the Galactic reference sources, XTE J1550–564 (blue diamonds), H 1743–322 (pink squares), 4U 1630–47 (green stars) and GRS 1915+105 (brigh blue stars).

The best-fit parameters in the HSS state (right panel) are  $\Gamma = 2.77 \pm 0.02$ ,  $kT_s = 50 \pm 4$  eV,  $N = 7.2 \pm 0.6 L_{35}/d_{10}^2$  and  $\log(A) = 0.28 \pm 0.06$  [ $\chi_{red}^2 = 0.98$  for 265 degrees of freedom (dof)], while the best-fit model parameters for the IS state (central panel) are  $\Gamma = 2.6 \pm 0.2$ ,  $kT_s = 40 \pm 2$  eV,  $N = 4.3 \pm 0.9 L_{35}/d_{10}^2$  and  $\log(A) = -0.72 \pm 0.08$  [ $\chi_{red}^2 = 0.93$  for 215 dof]; and, finally, the best-fit model parameters for the LHS state (left panel) are  $\Gamma = 1.7 \pm 0.3$ ,  $kT_s = 120 \pm 6$  eV,  $N = 0.19 \pm 0.05 L_{35}/d_{10}^2$  and  $\log(A) = -0.24 \pm 0.08$  [ $\chi_{red}^2 = 1.06$  for 237 dof]. A systematic uncertainty of 1% is intended to represent the instrumental flux calibration uncertainty and has been applied to all analyzed *Swift* spectra.

Analysis of the *Swift*/XRT data fits (see Figure 5) showed that  $\Gamma$  monotonically increases from 1.5 to 2.8, when the normalization of the spectral component (or  $\dot{M}$ ) increases by a factor about 5.

#### 4. A BH mass estimate of the OJ 287 secondary

Now, we use the scaling method for our estimate of the BH mass,  $M_{OJ287}$ . Beforehand we do not know what kind of a BH mass can be estimated using our data for OJ 287. The BH mass using the scaling method applies the  $\Gamma - N$  correlation (see ST09 for details). This method comes to (i) identifying for a pair of BHs for which the  $\Gamma$  correlates with increasing normalization  $N$  (which is proportional to mass accretion rate  $\dot{M}$  and a BH mass  $M$ , see ST09, Eq. (7)) and the saturation level,  $\Gamma_{sat}$  are the same and (ii) calculating the scaling coefficient  $s_N$  which allows us to determine a BH mass of the target object. We also should emphasize that one needs a ratio of distances for the target and reference sources in order to estimate a BH mass using the following equation for the scaling coefficient

$$s_N = \frac{N_r}{N_t} = \frac{m_r d_t^2}{m_t d_r^2} f_G \quad (3)$$

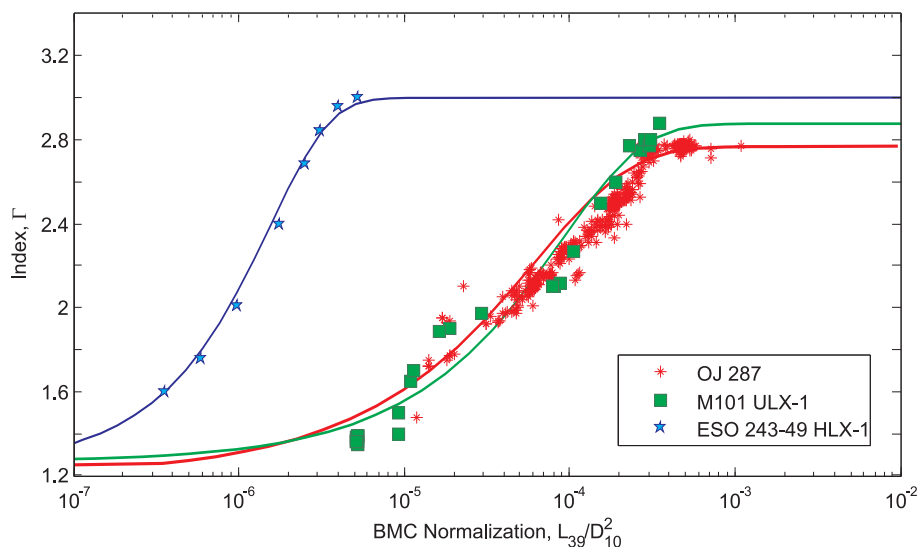


**Fig. 7.** Scaling of the photon index  $\Gamma$  versus the normalization  $N$  for OJ 287 (red line – target source) using  $\Gamma - N$  correlations for extragalactic sources, ESO 243–49 HLX–1 and M101 ULX–1 (blue and green points).

where  $N_r$ ,  $N_t$  are normalizations of the spectra,  $m_t = M_t/M_\odot$ ,  $m_r = M_r/M_\odot$  are the dimensionless BH masses with respect to solar,  $d_t$  and  $d_r$  are distances to the target and reference sources, correspondingly. A geometrical factor,  $f_G = \cos i_r / \cos i_t$  where  $i_r$  and  $i_t$  are the disk inclinations for the reference and target sources, respectively [see ST09, Eq. (7)].

We found that XTE 1550–564, H 1743–322, 4U 1630–47, GRS 1915+105, ESO 243–49 and M101 ULX–1 can be used as the reference sources because these sources met all aforementioned requirements to estimate a BH mass of the target source OJ 287 [see items (i) and (ii) above].

In Figure 6 we demonstrate how the photon index  $\Gamma$  evolves with normalization  $N$  (proportional to the mass accretion rate  $\dot{M}$ ) in the Galactic source XTE 1550–564 and OJ 287 where  $N$  is presented in the units of  $L_{39}/d_{10}^2$  ( $L_{39}$  is the source luminosity in units of  $10^{39}$  erg/s and  $d_{10}$  is the distance to the source in units of 10 kpc).

As we show in Fig. 7 that the correlations  $\Gamma$  vs  $N$  are self-similar for the target source (OJ 287) and two M101 ULX–1 and ESO 243–49 HLX–1 are ultraluminous X-ray sources. Moreover, these three sources have almost the same index saturation level  $\Gamma$  about 2.8. We estimated a BH mass for OJ 287 using the scaling method (see e.g. ST09). In Figure 6 we illustrate how the scaling method works shifting one correlation vs another. From these correlations we could estimate  $N_t$ ,  $N_r$  for OJ 287 and for the reference sources (see Table 2). A value of  $N_t = 2.4 \times 10^{-4}$ ,  $N_r$  in units of  $L_{39}/d_{10}^2$  is determined in the beginning of the  $\Gamma$ -saturation part [see Figs. 6 and 7, ST07, ST09, Seifina et al. (2014); Titarchuk & Seifina (2016a,b, 2009)].

A value of  $f_G = \cos i_r / \cos i_t$  for the target and reference sources can be obtained using inclination for OJ 287  $i_t = 50^\circ$  and for  $i_r$  (see Table 2). As a result of the estimated target mass (OJ 287),  $m_t$  we find that

$$m_t = f_G \frac{m_r d_t^2}{s_N d_r^2} \quad (4)$$

where we use values of  $d_t = 1.073$  Gpc .

Applying Eq.(4), we can estimate  $m_t$  (see Table 2) and we find that the secondary BH mass in OJ 287 is about  $1.25 \times (1 \pm 0.18) \times 10^8$  solar masses. To obtain this estimate with appropriate error bars we need to consider error bars for  $m_r$  and  $d_r$  assuming

in the first approximation, errors for  $m_r$  and  $d_r$  only. We rewrote Eq. (4) as

$$m_t(1 + \Delta m_t/m_t) = f_G \frac{m_r d_t^2}{s_N d_r^2} (1 + \Delta m_r/m_r)(1 + 2\Delta d_r/d_r). \quad (5)$$

Thus we obtained errors for the  $m_t$  determination (see Table 2, second column for the target source) that

$$\Delta m_t/m_t \sim \Delta m_r/m_r + 2\Delta d_r/d_r. \quad (6)$$

In order to calculate the dispersion  $\mathcal{D}$  of the arithmetic mean  $\bar{m}_t$  for a BH mass estimate using different reference sources  $\mathcal{D}$  (see Table 2), one should keep in mind that

$$\mathcal{D}(\bar{m}_t) = D/n \quad (7)$$

where  $D$  is the dispersion of  $m_r$  using each of the reference source and  $n = 6$  is a number of the reference sources. As a result we obtained that the mean deviation of the arithmetic mean

$$\sigma(\bar{m}_t) = \sigma / \sqrt{n} \sim 0.18 \quad (8)$$

and finally we came to that (see also Table 2)

$$\bar{m}_t \sim 1.25 \times (1 \pm 0.18) \times 10^8 \text{ solar masses.} \quad (9)$$

It should be noted that in our calculations we assume the angle between the normal to the secondary disk and the line of sight to be about 50 degrees. However, this angle may be different. In fact, Dey et al. (2021) and Valtonen et al. (2021) argued that one should see the secondary disk almost face-on, namely, this angle  $i_t$  is about zero. Consequently the mass of the secondary should then be slightly lower,  $\bar{m}_t \sim 0.8 \times 10^8$  solar masses.

## 5. Power density spectrum

In Figure 8 we presented evolution of the power density spectrum of OJ 287 with bintime of 4000 s using *RXTE*/ASM data from 1997 to 2015 in 0.3–12 keV energy range. We made PDSs in the range of  $10^{-7} - 10^{-4}$  Hz frequency and subtracted the contribution because to Poissonian statistics. As it is seen from this Figure the PDS undergoes temporal evolution. If in the upper

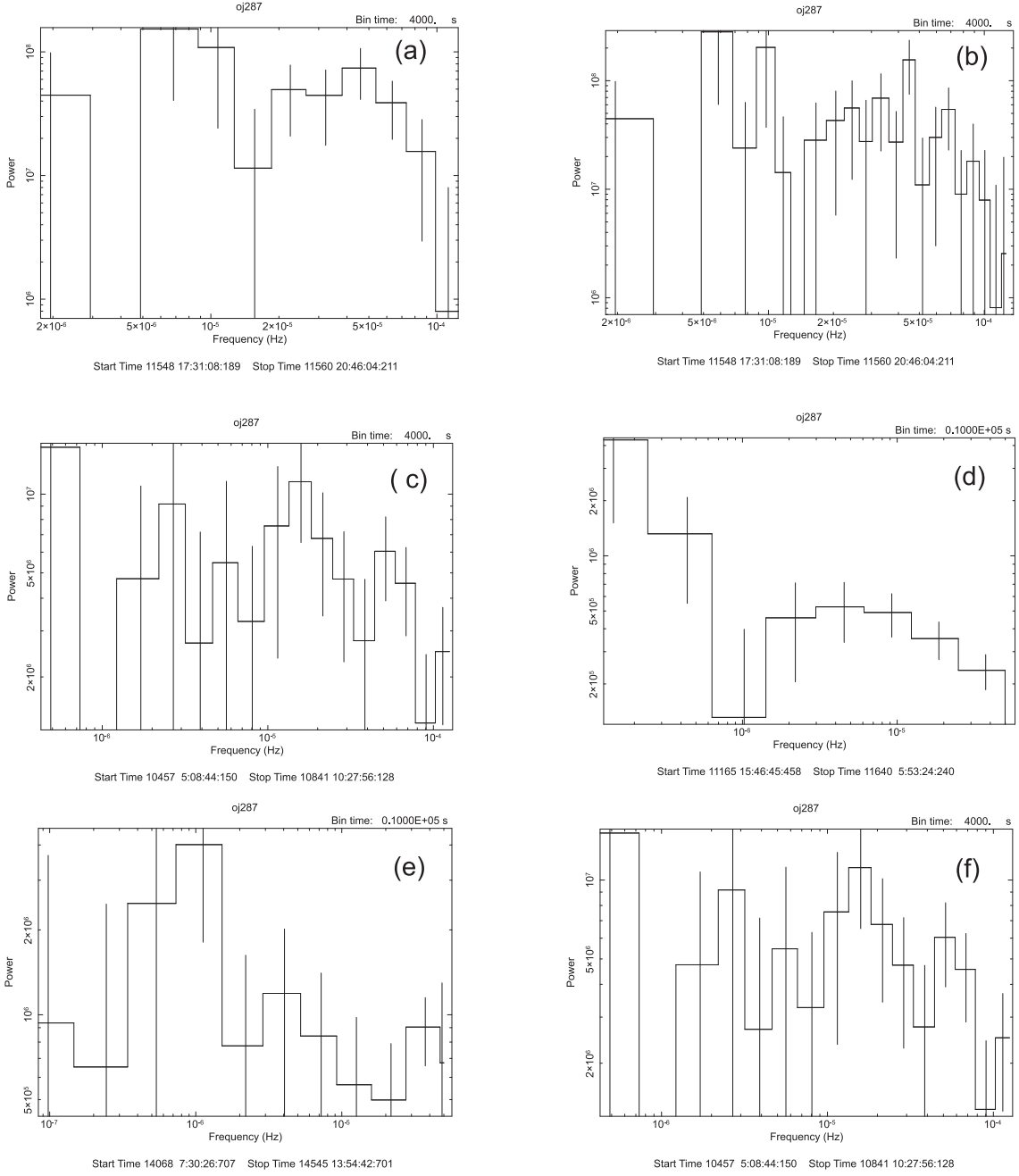


**Fig. 8.** Evolution of the power density spectrum of OJ 287 with time. It is clearly seen the PDS evolution with the characteristic peaks in the range of  $10^{-6}$  and  $10^{-5}$  Hz.

plot we see a wide plateau from  $7 \times 10^{-6}$  to  $10^{-5}$  Hz, while in the lower panel it takes place in much wider of frequency range from  $10^{-6}$  to  $10^{-5}$  Hz. We can evaluate the size of the Compton cloud (CC) emitting the emergent spectra using the presented plateaus. The characteristic frequency of these plateaus  $\nu_{plat}$  can be estimated as

$$\nu_{plat} \sim V_{plas}/L_{CC} = 1.4 \times 10^8 \frac{V_{plas}/(10^8 \text{ cm s}^{-1})}{L_{CC}(\text{cm})} \text{ cm s}^{-1}, \quad (10)$$

where  $L_{CC}$  is the CC size and  $V_{plas} = 1.4 \times 10^8 \text{ cm s}^{-1}$  is a typical plasma (proton) velocity in the CC related to the plasma temperature of order of 10 keV [see e.g. Shaposhnikov & Titarchuk (2009)]. We use a frequency  $\nu_{plat} \sim 10^{-5}$  Hz in order to estimate

the CC size:

$$L_{CC} \sim 1.4 \times 10^{13} \frac{V_{plas}/10^8 \text{ cm s}^{-1}}{\nu_{plat}/10^{-5} \text{ Hz}} \text{ cm}. \quad (11)$$

Using this CC size  $L_{CC}$  one can easily estimate the appropriate BH mass:

$$M_{OJ287} \sim L_{CC}/R_{S\odot} \sim 10^8 \text{ solar masses}, \quad (12)$$

which is, by order of magnitude, close to our BH mass value using the  $\Gamma$ - mass accretion rate correlation [see Eq. (9), Table 2 and Fig. 7].

## 6. Discussion

In the previous chapter using the power spectra (see Figure 8) we estimated the CC size as  $L_{CC} \sim 1.4 \times 10^{13}$  cm where the X-

ray emergent spectrum was formed. Applying this value of  $L_{CC}$  we confirmed a BH mass value of order  $10^8$  solar masses found using the  $\Gamma$ – mass accretion rate correlation (see Table 2, Figs. 6–7, and section 4). This type of the CC, with  $L_{CC}$  of order of  $10^{13}$  cm is definitely not related to a BH mass of order of  $10^{10}$  as KOM21 claimed.

KOM21 also noted that their inferred X-ray luminosity with respect to the Eddington one  $L_x/L_{Edd} < 6 \times 10^{-4}$  was too small for  $M_{BH, primary} \sim 1.8 \times 10^{10} M_\odot$ . Furthermore, they mentioned, in their section 4.3 a possibility that  $L_{x, iso} = 1.3 \times 10^{45}$  erg  $s^{-1}$  can be associated with the secondary of a BH mass  $M_{BH, secondary} \sim 1.5 \times 10^8 M_\odot$ . In KOM21 the authors presented a profound spectral evolution from the low to high states (see their Figs. 4–7). They correctly claimed using their spectral results that all spectral states observed in OJ 287 in the 0.3–10 keV band evolved from rather flat to ultra-steep ( $\Gamma_x = 1.5 - 2.8$ ). We confirmed this kind of spectral behavior in our Figures 4–5 that  $\Gamma$  significantly evolved depending on Normalization (proportional to the mass accretion rate) from 1.5 to 2.8 too.

One can argue that we did not realize, that the emission from this BL Lac object, comes from a jet. In fact, we do not see any serious arguments for this statement. A particularly important point regards the fitting of *Swift* X-ray spectra. One can think that our spectral models contains too many components and thus cannot fit to low-resolution *Swift* data, since there are then much more free parameters than actual independent data bins. This is not the case because our continuum spectral model is an XSPEC model consisting of the Comptonization (BMC) component. The spectral model parameters are the equivalent hydrogen absorption column density  $N_H$ ; the photon index,  $\Gamma$ ;  $\log(A)$  is related to the Comptonized factor  $f$ ; the color temperature and normalization of the seed photon blackbody component,  $kT_s$  and  $N$ , respectively. One can claim that simple power-law models are appropriate for *Swift* spectral fitting. However, it is important to emphasize that a power-law itself is not a physical model but if one considers any up-scattering model (or just a particle acceleration) in the energetic cloud, which a particle energy is much greater than that of photons, then a power-law is formed (see a proof of this statement in ST09).

In the light of the obtained results, we can take an updated look at the discrepancy between the BH mass in the nucleus of the M87 galaxy, obtained using different methods. Namely, the discrepancy in the estimates of the BH mass in M87 ( $3.5 - 6.5 \times 10^9 M_\odot$  [from its EHT radio image (Akiyama et al. 2019) and based on the gas dynamic analysis (Walsh et al. 2013; Akiyama et al. 2019) and stellar dynamics of M87 (Akiyama et al. 2019) using long-term optical observations (Gebhardt et al. 2011)] and  $6.5 \times 10^7 M_\odot$  (by the method BH mass scaling from X-ray data (Titarchuk et al. 2020). Titarchuk et al. (2020) reduced the BH mass in M87 by a factor of 100 compared to standard methods (Gebhardt et al. 2011; Walsh et al. 2013; Akiyama et al. 2019), using the timing analysis of the X-ray variability in M87. This discrepancy is difficult to explain only due to different ranges of radiation energy observations. Assuming that M87 contains a binary BH at its center (Emami & Loeb 2020; Davelaar & Haiman 2022; Dou et al. 2022), an estimate of the BH mass by analyzing the power spectrum of M87 using a characteristic variability time of  $5 \times 10^{-7}$  s yields an estimate of the CC size in M87 of  $L_{CC} \sim 2 \times 10^{13}$  cm and the BH mass of  $(6.5 \pm 0.5) \times 10^7 M_\odot$ . At the same time, these two SMBHs can be distinguished only by the scale of variability. In terms of this approach, it is possible that the BH mass measurement in M87 by Titarchuk et al. (2020) refers specifically to the BH of smaller mass (secondary), in contrast to the approach of the gas

and stellar dynamics as well as the EHT image analysis methods for an estimate of the primary BH mass or the total (primary + secondary) BH mass. This can be considered as a possible observational indication of the presence of a BH binary in M87.

Recently, Ning Jiang and his colleagues (Jiang et al. 2022) pointed out a similar picture of BH duality in the active galaxy nuclear. Namely, they argued for the probable presence of a BH binary in the Seyfert galaxy SDSSJ143016.05+230344.4. Dou et al. (2022) indicated that in this binary system, consisting of two SMBHs of different masses, a decay of the orbital period was observed, which confirms the initial hypothesis of the presence of an eccentric SMBH binary in the center of this galaxy.

## 7. Conclusions

The multi-wavelength outburst activity in OJ 287 with the X-ray telescope onboard the *Swift* made a lot of questions whether the source contains one or two BHs. It is very important to reveal the characteristics of this binary. In the presented paper we demonstrated that the OJ 287 X-ray spectra underwent the state transition from the LHS to the IS and then to the HSS (see Fig. 4). We obtained that energy spectra in all spectral states can be modeled using a product of the wabs and a BMC Comptonization component.

Moreover, we discover in OJ 287 the correlation of the index  $\Gamma$  with normalization,  $N$  (proportional to the disk mass accretion rate  $\dot{M}$ , see Fig. 7) similar to those established in BH Galactic sources by ST09. We found that  $\Gamma$  increases monotonically with  $\dot{M}$  from the LHS to IS and HSS, and then saturates at  $\Gamma \sim 2.8$ . This can be considered as observational evidence of the presence of a BH in OJ 287. Based on this correlation, we apply the scaling method of ST09 to estimate a BH mass is about  $1.25 \times 10^8$  solar masses, using the well-studied Galactic X-ray BHs, XTE 1550–564, H 1743–322, 4U 1630–47, GRS 1915+105 and extra-galactic BHs ESO 243–49 and M101 ULX–1 as reference sources.

Also using the power spectrum analysis we inferred the size of the Compton cloud  $L_{CC} \sim 10^{13}$  cm where X-ray spectra were formed. Using this value of  $L_{CC}$  we confirmed that a BH mass of the secondary in OJ 287 was of order of  $10^8$  solar masses consistent with the index,  $\Gamma$ –correlation (the scaling method) with respect to the mass accretion rate.

## Acknowledgements

We acknowledge support from UK *Swift* Science Data Centre at the University of Leicester for supplied data. We thank the anonymous referee for the careful reading of the manuscript and for providing valuable comments.

## Data availability

This research has made using the data and/or software provided by the High Energy Astrophysics Science Archive Research Center (HEASARC), which is a service of the Astrophysics Science Division at NASA/GSFC and the High Energy Astrophysics Division of the Smithsonian Astrophysical Observatory. The data used in this paper are public and available through the GSFC public archive at <https://heasarc.gsfc.nasa.gov>. This work was made use of XRT and BAT data supplied by the UK *Swift* Science Data Centre at the University of Leicester<sup>2</sup>.

<sup>2</sup> [https://www.swift.ac.uk/swift\\_portal](https://www.swift.ac.uk/swift_portal)

## References

- Akiyama, K. et al. 2019, *ApJL*, 875, L6
- Begelman, M. C., Blandford, R. D. & Rees, M. J. 1980, *Nature*, 287, 307
- Borozdin, K., Revnivtsev, M., Trudolyubov, S. et al., 1999, *ApJ*, 517, 367
- Chan, C.-H., Piran, T., Krolik, J. H. 2021, *ApJ*, 914, 107
- Charisi, M. et al. 2016, *MNRAS*, 463, 2145
- Chen, Y.-C. et al. 2020, *MNRAS*, 499, 2245
- Ciprini S. et al., 2007, *Mem. S. A. It.*, 78, 741
- Davelaar, J., Haiman, Z., 2022, *Phys. Rev. Lett.*, 128, 191101
- Dey, L., Valtonen, M.J., Gopakumar, A. et al. 2019, *MNRAS*, 503, 4400
- Dey, L., Gopakumar, A., Valtonen, M. et al. 2019, *Univ.* 5, 108
- Dou, L., Jiang, N., Wang, T. et al., 2022, *A&A* 665, L3
- Gebhardt, K., Adams, J., Richstone, D., et al. 2011, *ApJ*, 729, 119
- Graham, M. J. et al. 2015, *MNRAS*, 453, 1562
- Gómez, G.L., Traianou, E., Krichbaum, T.P., Lobanov, A. P., Fuentes, A. et al. 2022, *ApJ*, 924, 122
- Gupta S. P., et al., 2012, *New Astron.*, 17, 8
- Emami, R. & Loeb, A., 2020, *MNRAS*, 495, 536
- Evans, P. A., Beardmore, A. P., Page, K. L., et al. 2009, *MNRAS*, 397, 1177
- Evans, P.A. et al. 2007, *A&A*, 469, 379
- Jiang, N., Yang, H., Wang, T. et al., 2022, *Nature*, *astro-ph/2201.11633*
- Komossa, S., et al., 2021, *MNRAS*, 504, 5575
- Laine, S., Dey, L., Valtonen, M. et al. 2020, *ApJL*, 894, L1
- Laurent, P., & Titarchuk, L. 1999, *ApJ*, 511, 289
- Laurent, P., & Titarchuk, L. 2011, *ApJ*, 727, 34
- Liu, T. et al. 2016, *ApJ*, 833, 6
- Orosz, J. A. et al. 2002, *ApJ*, 568, 84
- Sagar R., Stalin C. S., Gopal-Krishna, Wiita P. J., 2004, *MNRAS*, 348, 176
- Sanchez-Fernandez, C., Castro-Tirado, A. J., Duerbeck, H.W., et al. 1999, *A&A*, 348, L9
- Seifina, E., Titarchuk, L. & Ugolkova, L. 2018, *A&A*, 619, 217
- Seifina, E., Chekhtman, A. & Titarchuk, L. 2018, *A&A*, 613, 48
- Seifina, E., Titarchuk, L., & Virgili, E. 2017, *A&A*, 607, A38
- Seifina, E., Titarchuk, L., & Shaposhnikov, N. 2016, *ApJ*, 821, 23
- Seifina, E. Titarchuk, L. & Shaposhnikov, N. 2014, *ApJ*, 789, 57
- Seifina, E., & Titarchuk, L. 2011, *ApJ*, 737, 128
- Seifina, E. & Titarchuk, L. 2010, *ApJ*, 722, 586
- Shaposhnikov, N., & Titarchuk, L. 2009, *ApJ*, 699, 453 (ST09)
- Shaposhnikov, N., & Titarchuk, L. 2007, *ApJ*, 663, 449
- Shakura, N.I., & Sunyaev, R.A. 1973, *A&A*, 24, 337 (SS73)
- Shi, W., Liu, X. & Song, H., 2007, *Ap&SS*, 310, 59
- Sillanpaa A. et al., 1988, *ApJ*, 325, 628
- Sobczak, G. J., McClintock, J. E., Remillard, R. A., & Bailyn, C. D. 1999, *ApJ*, 520, 776
- Sobolewska M. A. & Papadakis, I.E. 2009, *MNRAS*, 399, 1997
- Titarchuk, L.G. & Fiorito, R. 2004, *ApJ*, 612, 988
- Titarchuk, L. & Seifina, E. 2021, *MNRAS*, 501, 5659
- Titarchuk, L., Seifina, E., Chekhtman, A. & Ocampo, I. 2020, *A&A*, 633, A73
- Titarchuk, L. & Seifina, E. 2017, *A&A*, 602, 113
- Titarchuk, L. & Seifina, E. 2016a, *A&A*, 585, 94, 2
- Titarchuk, L. & Seifina, E. 2016b, *A&A*, 595, 110
- Titarchuk, L. & Seifina, E. 2009, *ApJ*, 701, 1463
- Titarchuk, L., Shaposhnikov, N. & Seifina, E. 2010, *AIP Conference Proceedings*, 1205, 168
- Titarchuk, L.G., Mastichiadis, A. & Kylafis, N.D. 1997, *ApJ*, 487, 834
- Titarchuk, L. & Zannias, T. 1998, *ApJ*, 499, 315
- Valtonen, M.J., Dey, L., Gopakumar, A. et al. 2021, *Galaxy*, 10, 1
- Valtonen, M., Ciprini, S. & Pihajoki, P. 2012, *MNRAS*, 427, 77
- Valtonen M. J. et al., 2010, *Celest. Mech. Dyn. Astron.*, 106, 235
- Valtonen M. J. et al., 2006, *ApJ*, 646, 36
- Walsh, J. L., Barth, A. J., Ho, L. C., & Sarzi, M. 2013, *ApJ*, 770, 86
- Wilms, J., Allen, A., McCray, R. 2000, *ApJ*, 542, 914
- Zheng, Z.-Y. et al. 2016, *ApJ*, 827, 56